1. Shaik Ruksana Begam[1,2], 2. Loveswara Rao Burthi[1], 3. Shobha Rani Depuru[2]

Koneru Lakshmaiah Education Foundation (1), Institute of Aeronautical Engineering (2)
ORCID: 1. 0000-0001-5161-4086; 2. 0000-0002-1094-2208; 3. 0000-0001-8235-9671

Regenerative Braking in Electric Vehicles using BLDC motor with Modified Torque and Adaptive-Neuro-Fuzzy-Control

Abstract. In present days conventional vehicles were replaced by electric vehicles due to their low maintenance and eco-friendly nature with PMBLDCM motor due to its simple design, long-term usage, low noise, speed response, stability, and high efficiency. In electric vehicles, the speed control method is still difficult with PMBLDC motor to produce the desired high torque and to deal with uncertainty problems due to dynamic loads which cannot apply in conventional vehicles. To overcome these problems, we proposed the usage of Adaptive Neuro-Fuzzy Sliding Mode Control (ANF-SMC) which also handles electromagnetic torque (EMT), back EMF and stator current, nonlinear and uncertainties in the electric propulsion subsystem of electric vehicles by applying adaptive neuro-fuzzy sliding mode control for effective speed regulation and parameter tuning of the fuzzy system based on performance index of PMBLDC motor in the absence, presence and variable speed conditions. The simulation was done using the designed approach with MATLAB/Simulink R2020b with a Fuzzy tool kit and the performance of the proposed controller was compared with existing PID, SMC, FSMC, and AFSMC controllers to validate its success in improving the system characteristics. Simulation results infer that the proposed ANF-SMC controller with no overshoot and less rise, peak, and settling time than that of existing systems under different loads and variable speed conditions.

Streszczenie. W dzisiejszych czasach konwencjonalne pojazdy zostały zastąpione pojazdami elektrycznymi ze względu na ich niskie koszty utrzymania i przyjazny dla środowiska charakter z silnikiem PMBLDCM ze względu na prostą konstrukcję, długotrwałe użytkowanie, niski poziom hałasu, reakcję na prędkość, stabilność i wysoką wydajność. W pojazdach elektrycznych metoda kontroli prędkości w przypadku silnika PMBLDC jest nadal trudna do wytworzenia pożądanego wysokiego momentu obrotowego i poradzenia sobie z problemami niepewności wynikającymi z obciążeń dynamicznych, których nie można zastosować w pojazdach konwencjonalnych. Aby przezwyciężyć te problemy, zaproponowaliśmy zastosowanie adaptacyjnego neuro-rozmytego trybu ślizgowego (ANF-SMC), który obsługuje również moment elektromagnetyczny (EMT), wsteczne pole elektromagnetyczne i prąd stojana, nieliniowość i niepewności w podukładzie napędu elektrycznego pojazdów elektrycznych poprzez zastosowanie adaptacyjne sterowanie trybem neuro-rozmytego przesuwania w celu skutecznej regulacji prędkości i dostrajania parametrów systemu rozmytego w oparciu o wskaźnik wydajności silnika PMBLDC w warunkach nieobecności, obecności i zmiennej prędkości. Symulację przeprowadzono przy użyciu zaprojektowanego podejścia przy użyciu MATLAB/Simulink R2020b z zestawem narzędzi Fuzzy, a wydajność proponowanego sterownika porównano z istniejącymi sterownikami PID, SMC, FSMC i AFSMC, aby potwierdzić jego skuteczność w poprawie charakterystyki systemu. Z wyników symulacji wynika, że proponowany sterownik ANF-SMC nie charakteryzuje się przeregulowaniami i krótszym czasem narastania, szczytu i stabilizacji w porównaniu z istniejącymi systemami przy różnych obciążeniach i warunkach zmiennej prędkości. (Hamowanie regeneracyjne w pojazdach elektrycznych z wykorzystaniem silnika BLDC ze zmodyfikowanym momentem obrotowym i sterowaniem adaptacyjnym Neuro-Fuzzy)

Keywords: Regenerative Braking, Timer Diagram, Modified Torque, Battery State of Charge.
Słowa kluczowe: Hamowanie regeneracyjne, diagram czasowy, zmodyfikowany moment obrotowy, stan naładowania akumulatora

1. Introduction

Electric Vehicles were the promising replacement for internal combustion engines (ICE) with battery and motor technology [1] advancement. In electric vehicles [2] utilization of the battery efficiently and control of the motor were major issues, problems were solved with the usage of a brushless direct control motor (BLDCM) with modified torque for controlling and modifying the regenerative braking system. During the regenerative braking process, BLDCM with direct torque control (DTC) will act as a generator which converts inertial to electric energy and generated energy was reused in braking and saving. As per the literature survey many papers published on regenerative braking techniques used in EVs [3 to 6], braking energy recovered as per the survey by using a regenerative braking system (RBS) without changing the mechanical braking system (MBS) in [7], RBS with HPSS [8 to 10], using DC-DC converter for boosting control [11, 12], using battery capacitor with UC [13], using hybrid energy storage devices [14, 15]. In the case of recovering braking energy as mentioned have limitations such as more complicated designing controllers, maintenance cost and much lower back EMF generation.

2. Methodology
2.1 Circuit Diagram of Regenerative Braking System (CDRBS)

The Circuit Diagram of RBS (CDRBS) used in the proposed system represented in Fig.1, consists of the Battery State of Charge (BSOC), Battery used, six switches (S1 to S6), BLDCM motor and output (Rotor Angle, Speed and EMT). Proposed RBS designed with MATLAB/Simulink

with TSFIS, BSOC in regenerative system conducted with conventional DTC with PID (CPID), Modified DTC with PID (MPID), Modified DTC with Model Reference Adaptive System (MMRAS) and Modified DTC with Adaptive Neuro-Fuzzy Control System (ANFCS) controllers [16] and their comparative study described in the following section. Based on the voltage amplitude of the BLDCM motor rotor accurately synchronize with the motor speed guaranteed by the switch, so that the fault signal can be reduced. Implemented with MANFCS controller will adjust speed as per requirement. BLDCM motor operating with six switches S1 to S6 in six states of operation with an angle of 360^0 in one cycle.
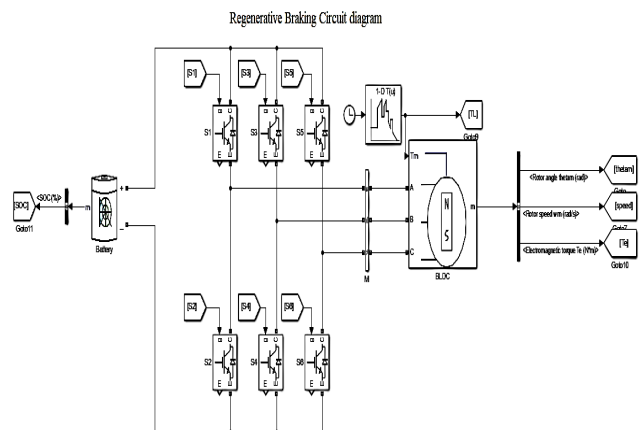

Fig. 1 Circuit Diagram of Regenerative Braking System (CDRBS)
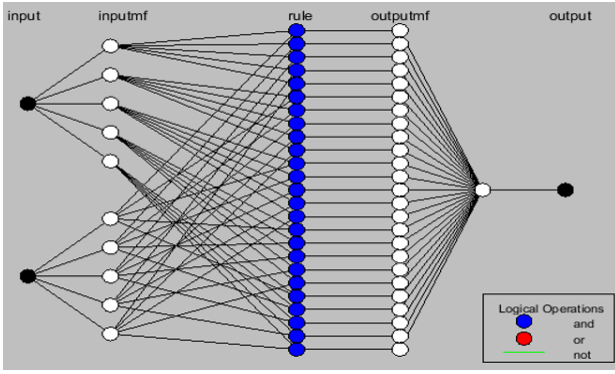
Fig. 2 Membership Functions and Fully Rules

Rotor speed (RS), stator current (SC), back-EMF and Electro Magnetic Torque (EMT) find out with MATLAB/Simulink software. For easy braking force distribution in electric vehicles by applying MANFCS using the force of brakes, SOC and speed as input. In this paper, MANFCS is applied by combining with NN for deriving learning ability with direct adjustments of functions and rules from the existing data. The architecture has five layers (fuzzification layer, rule layer, normalize firing strengths, consequence parameter sets and output layer) which are represented in Fig. 2.

2.1 Timer Diagram
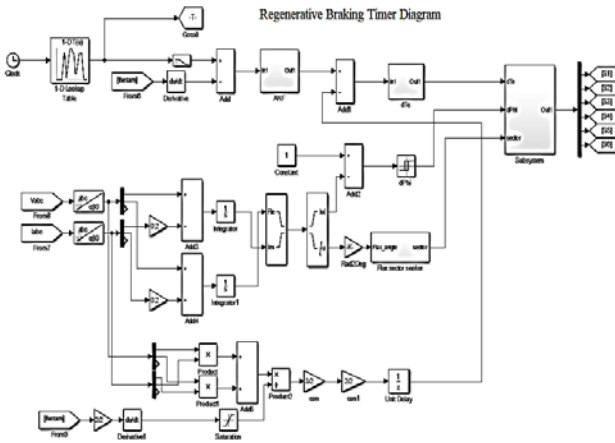
Fig. 3 Regenerative Braking Timer Diagram

In Fig. 3 Regenerative Braking Timer Diagram is described with a clock, lookup table, add operation and ANFC controller as input to get sub-systems of direct torque controls and six switches used in the proposed system.

3. Regenerative braking sub-systems for conventional DTC and modified DTC

In this work, both conventional and modified DTC driving systems were used for regenerative energy from braking by modifying the switching patterns which were shown in Fig. 4 and Fig. 5 the difference between these two sub-systems is BSOC with conventional and modified DTC. In modified regenerative braking DTC, the flux value of the stator will be greater than that of the flux value of the rotor, both stator and rotor fluxes have to be rotated in opposite directions for inverse torque generation. In the case of conventional DTC inverse torque cannot be generated.
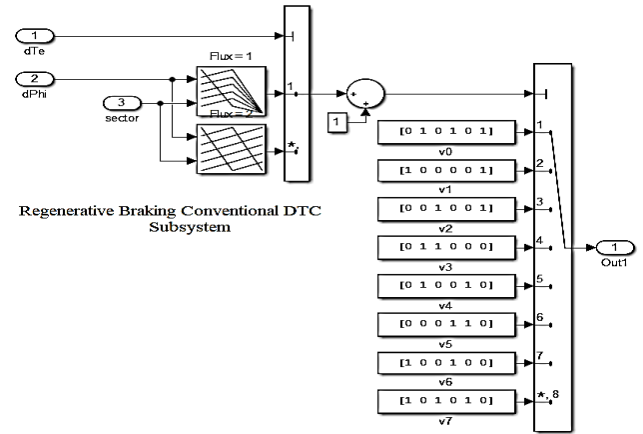

Fig. 4 Regenerative braking sub-systems for conventional Direct Torque Control (DTC)
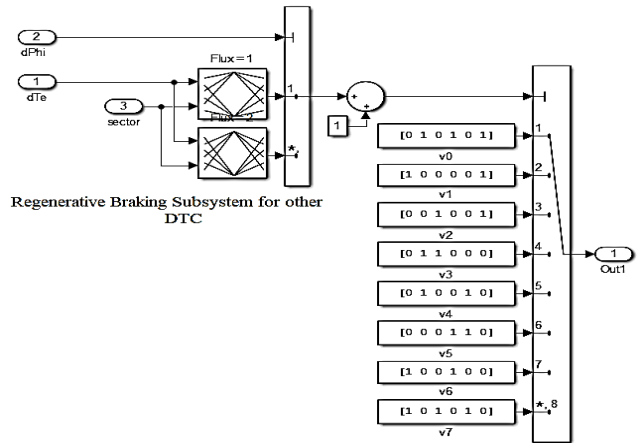

Fig. 5 Regenerative braking sub-systems for modified Direct Torque Control (DTC)

4. RESULTS and DISCUSSION
Conventional DTC with PID (CPID)

The state of charge (BSOC), Speed and Torque with PID controller under conventional torque were represented in the form of line diagrams from Fig. 6 to Fig. 8 by taking time in seconds on the x-axis ranging from 0 to 1.2 for all results, whereas 90.2 to 100 for SOC, 0 to 60 for speed, 0 to 35 for torque. As in the case of SOC initially, it starts with 100 (it will be up to 0.3 sec) as time increases its value decreases. In the case of rotor speed with reference speed up to 0.3 sec, it will be zero (rad/sec) and it will rise to 40 (rad/sec) within the time of 0.2 seconds, maintaining constant speed for a duration of 0.1 seconds later will be raised to 55(rad/sec) within 0.1 sec and will be maintained for 0.1 sec and later speed decreases gradually as time increases under conventional direct torque. In the case of electromagnetic torque with reference torque up to 0.3 sec, it will be common 0 N-m for both the cases, with a slight difference in time torque will rise to 23 N-m, later with no difference in time torque raise to 33 N-m. later as time increases there will be fluctuations in torque and will decrease as time increases under conventional direct torque.
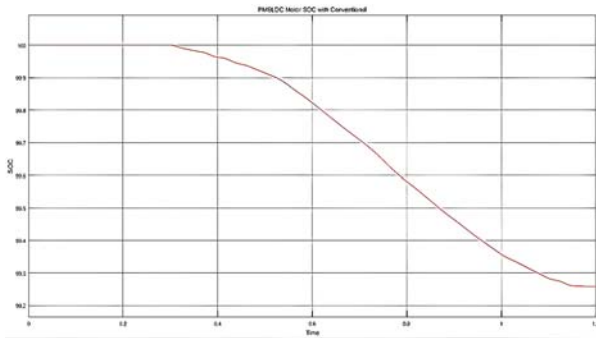
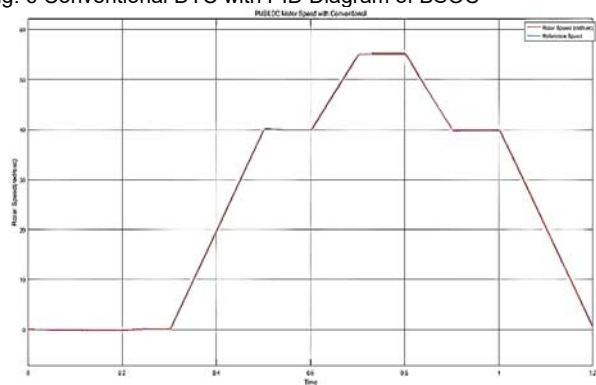Fig. 6 Conventional DTC with PID Diagram of BSOC
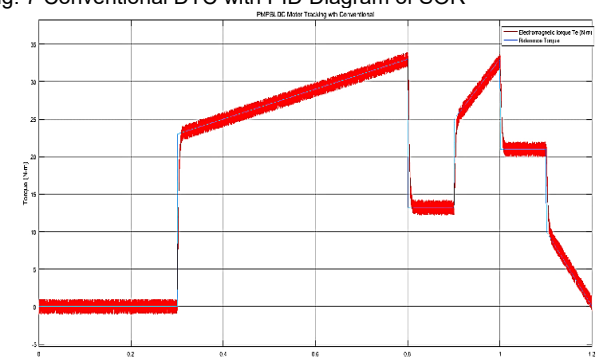

Fig. 7 Conventional DTC with PID Diagram of SOR

Fig. 8 Conventional DTC with PID Diagram of EMT

4.2 Modified DTC with PID (MPID)

The state of charge (SOC), Speed and Torque with PID controller under modified direct torque were represented in the form of line diagrams from Fig. 9 to Fig. 11 by taking time in seconds on the x-axis ranging from 0 to 1.2 for all results, whereas 99.4 to 100 for SOC, 0 to 6 for speed, -15 to 32 for torque. As in the case of SOC initially, it starts with 100 (it will be up to 0.3 sec) as time increases its value decreases continuously with consistency for every 0.1 sec up to 99.5 within 0.9 sec. In case of rotor speed up to 0.2 sec, it will be zero (rad/sec) and fluctuation in speed will occur from +6 (rad/sec) to -7 (rad/sec) within 0.9 sec and later it will rise to 40 (rad/sec) within time of 0.2 seconds, maintains constant speed for duration of 0.1 seconds later will be raised to 55(rad/sec) within 0.1 sec and will be maintained for 0.1 sec and later zero (rad/sec). In the case of electromagnetic torque with reference torque up to 0.3 sec, it will be common 0 N-m for both the cases, with a slight difference in time torque will rise to 22 N-m, later with no difference in time torque raise to 33 N-m. later as time increases there will be fluctuations in torque and will decrease up to -15 N-m as time increases under modified direct torque.
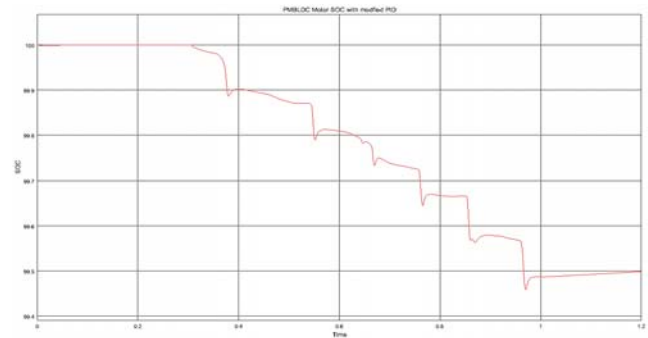

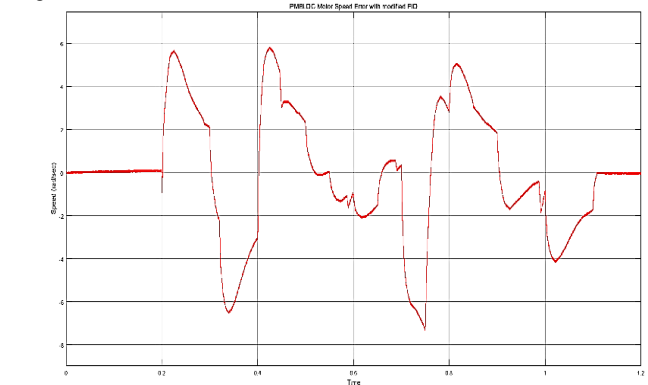Fig. 9 Modified DTC with PID Diagram of BSOC
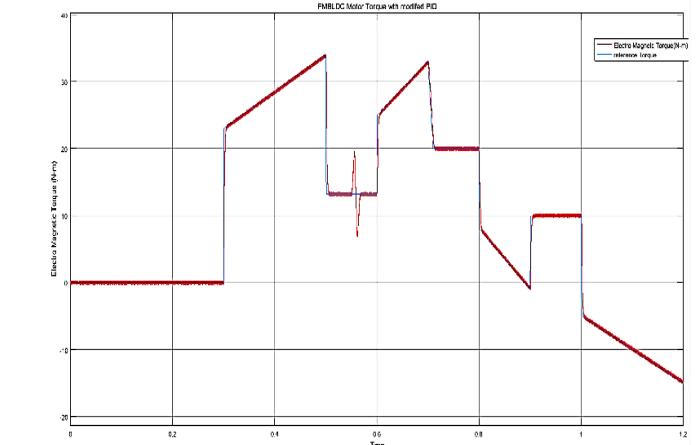

Fig. 10 Modified DTC with PID Diagram of SOR

Fig. 11 Modified DTC with PID Diagram of MTQ

Fig.12 represents switch S1 current in braking mode with time on the x-axis ranging from 0 to 1.2 sec and current in A ranging from -200 to +100. The current value will be zero A up to 0.3 sec and will fluctuate from 0.3 sec to 1.15 sec later it will be zero A.
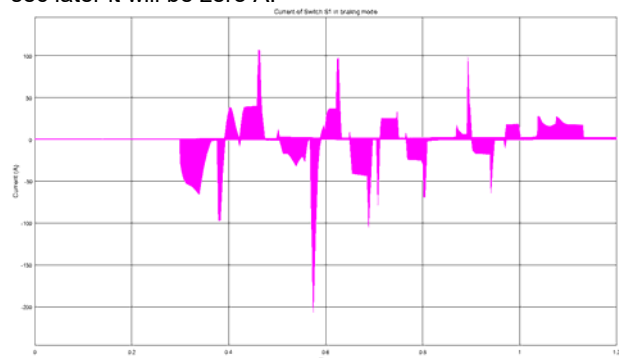

Fig. 12 Switch S1 current in braking mode

4.3 Modified MMRAS Controller

The state of charge (SOC), Speed and Torque with MMRAS controller under modified direct torque were

represented in the form of line diagrams from Fig. 13 to Fig. 15 by taking time in seconds on the x-axis ranging from 0 to 1.2 for all results, whereas 99.8 to 100 for SOC, 0 to 48 for speed, -15 to 32 for torque. As in the case of SOC initially, it starts with 100 (it will be up to 0.3 sec) as time increases its value decreases continuously with consistency for every 0.1 sec up to 99.9 within 0.9 sec. In case of rotor speed up to 0.2 sec it will be zero (rad/sec) and fluctuation in speed will occur from +48 (rad/sec) to 0 (rad/sec) within 0.9 sec and later with it will be 0 (rad/sec) within time of 0.2 seconds, maintains constant speed for duration of 0.1 seconds later will be raised to 48 (rad/sec) within 0.1 sec and will be maintained for 0.1 sec and later zero (rad/sec). In the case of electromagnetic torque with reference torque up to 0.3 sec, it will be common 0 N-m for both the cases, with a slight difference in time torque will rise to 22 N-m, later with no difference in time torque raise to 33 N-m. later as time increases there will be fluctuations in torque and will decrease up to -15 N-m as time increases under modified direct torque.
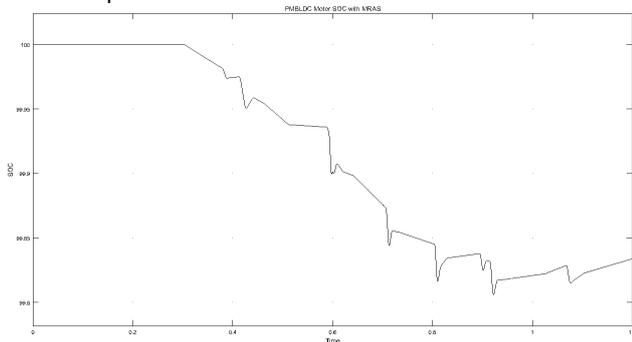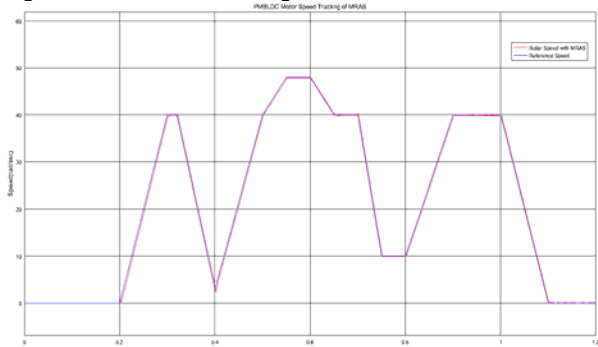

Fig. 13 Modified MMRAS Diagram of BSOC

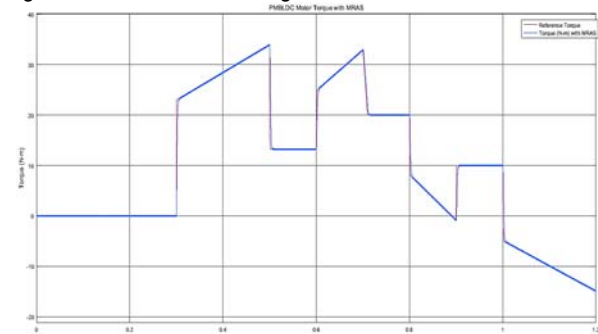Fig. 14 Modified MMRAS Diagram of SOR

Fig. 15 Modified MMRAS Diagram of MTQ

Figure 16 represents motor adaptive control with time on the x-axis ranging from 0 to 1.2 sec and motor adaptive control in kp ranging from 0 to +130. Motor Adaptive control value will be zero up to 0.3 sec and will increase from 0 to 130 from 0.3 sec to 1.0 sec later decreases to 120.
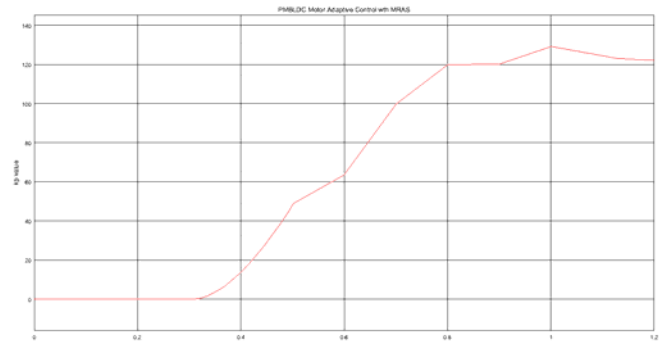

Fig. 16 Modified DTC with Model Reference Adaptive System (MMRAS) Diagram of Motor Adaptive Control

4.4 Modified DTC with Adaptive Neuro-Fuzzy Control System (MANFCS) controllers

The state of charge (SOC), Speed and Torque with MANFCS controller under modified direct torque were represented in the form of line diagrams from Fig. 17 to Fig. 19 by taking time in seconds on the x-axis ranging from 0 to 1.2 for all results, whereas 99.75 to 100 for SOC, 0 to 55 for speed, -15 to 32 for torque. As in the case of SOC initially, it starts with 100 (it will be up to 0.3 sec) as time increases its value decreases continuously with consistency for every 0.1 sec up to 99.75 within 0.9 sec. In case of rotor speed up to 0.3 sec it will be zero (rad/sec) and increases up to 40 (rad/sec) within the time of 0.2 seconds, maintains constant speed for a duration of 0.1 seconds later will increase up to 55 (rad/sec) maintain for one sec and later decrease gradually as time increases. In the case of electromagnetic torque with reference torque up to 0.3 sec, it will be common 0 N-m for both the cases, with a slight difference in time torque will rise to 22 N-m, later with no difference in time torque raise to 33 N-m. later as time increases there will be fluctuations in torque and will decrease up to -15 N-m as time increases under modified direct torque.
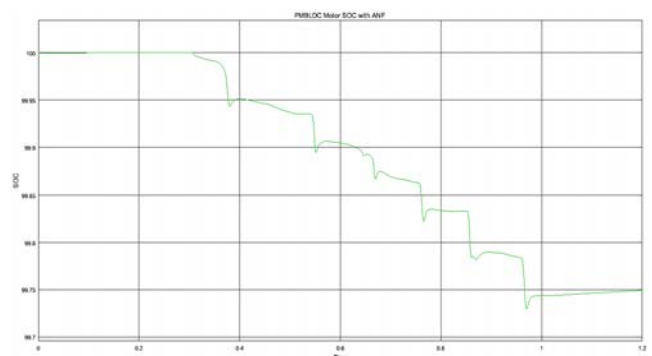

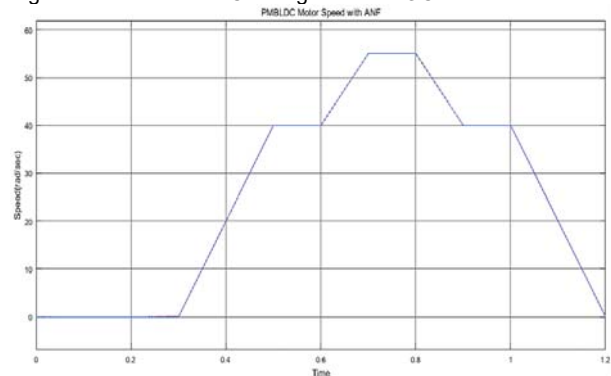Fig. 17 Modified MANFCS Diagram of BSOC

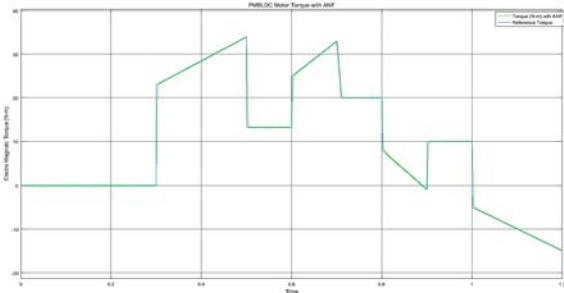Fig. 18 Modified MANFCS Diagram of SOR

Fig. 19 Modified MANFCS Diagram of MTQ

Fig. 20 represents speed reference tracking error with time on the x-axis ranging from 0 to 1.2 sec and motor speed reference error in (rad/sec) ranging from -0.5 to +0.5 (rad/sec). Speed reference tracking error will be zero up to 0.2 sec and will fluctuate values from -0.5 to +0.5 (rad/sec) from 0.2 sec to 1.1 sec later it will be zero.
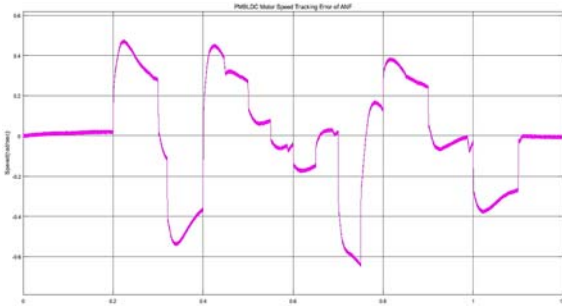

Fig. 20 Modified DTC with Adaptive Neuro-Fuzzy Control System (MANFCS) Diagram of Speed Reference Tracking Error

In Fig. 21 membership functions and surface views of Modified DTC with Adaptive Neuro-Fuzzy Control System (MANFCS) were represented from Fig. 21(a) to Fig. 21(d), in which Fig. 21(a) membership functions of input1, Fig. 21(b) with membership function of in2, Fig. 21(c) membership function of op, Fig. 21(d) surface view of input1, input2 and output.
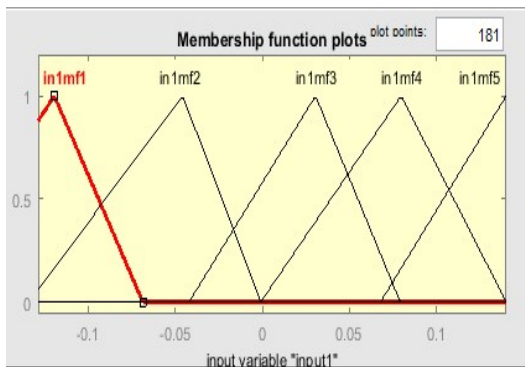
Fig. 21 (a) Modified MANFCS Diagram with Membership Function of in1
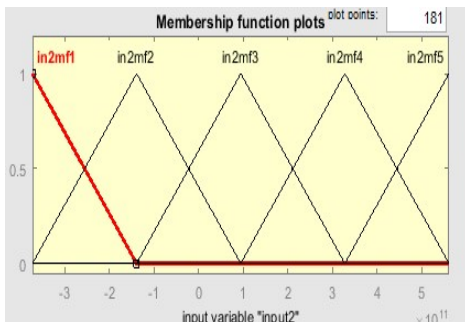
Fig. 21(b) Modified MANFCS Diagram with Membership Function
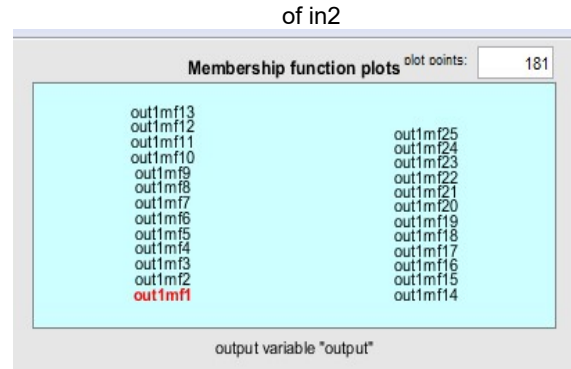
Fig. 21(c) Modified MANFCS Diagram with Membership Function of op
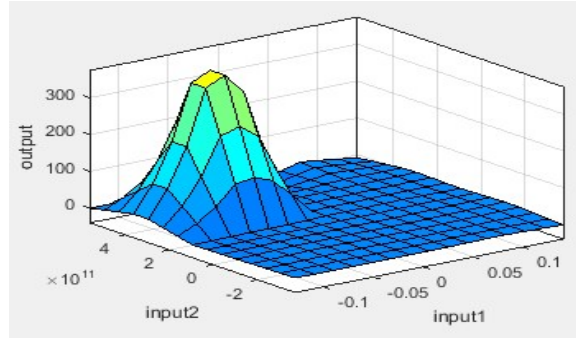
Fig. 21(d) Modified MANFCS Diagram with Surface View

Fig. 21 Modified DTC with Adaptive Neuro-Fuzzy Control System (MANFCS) membership and surface view diagrams

CPID with DTC   MPID with MDTC

MMRAS with MDTC   MANFCS with MDTC
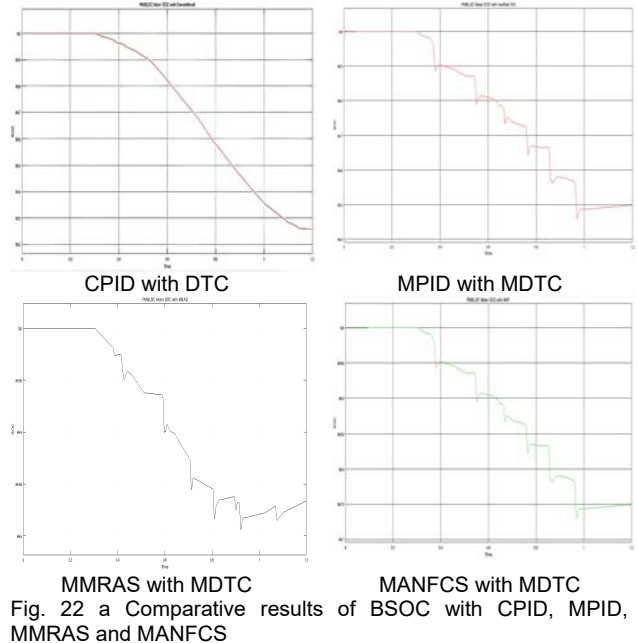
Fig. 22 a Comparative results of BSOC with CPID, MPID, MMRAS and MANFCS

5. Comparative Results of BSOC, SOR and EMT with four controllers

5.1 Comparative Results of BSOC with four controllers

The state of Charge (SOC) of the system varies with Direct and Modified Control and can be treated as the main difference among comparative results with various components, normally with slight differences in the case of speed and torque. SOC is the same for both direct and modified torque with all four controllers from 0 sec to 0.3 sec 100%, as time increases the SOC is greater in the proposed MANCS controller (100 % to 99.85%) than that of

the other three controllers, comparative results were shown in fig. 22a and Table 1. From the results in can be inferred that BSOC improved and as SOR increases there will be a considerable drop in BSOC by which the main purpose of the proposed MANCS controller which is to control and improve system performance was met.

TABLE 1 COMPARATIVE RESULTS OF BSOC WITH FOUR CONTROLLERS			
CPID with DTC		MPID with MDTC	
T in seconds	BSOC (%)	T in seconds	BSOC (%)
0 to 0.30	**100**	0 to 0.30	**100**
0.31 to 1.20	99.25	0.31 to 0.98	99.45
		0.99 to 1.20	99.50
MMRAS with MDTC		MANFCS with MDTC	
T in seconds	BSOC (%)	T in seconds	BSOC (%)
0 to 0.30	**100**	0 to 0.30	**100**
0.31 to 0.98	99.80	0.31 to 0.98	**99.83**
0.99 to 1.20	99.83	0.99 to 1.20	**99.85**

5.2 Comparative results of SOR with our controllers

CPID with DTC   MPID with MDTC
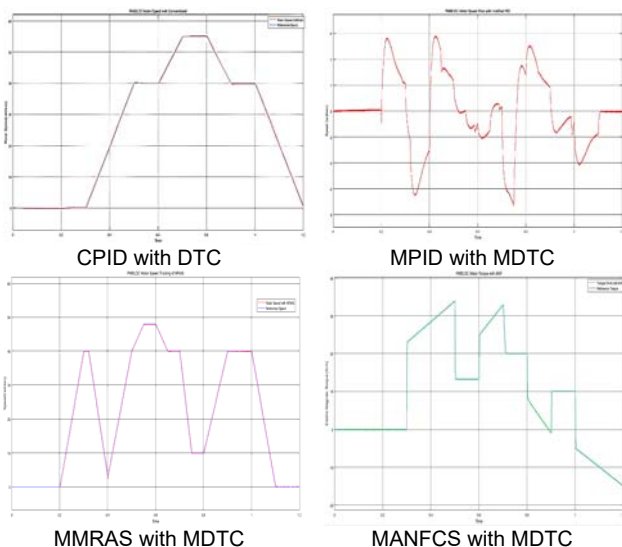
MMRAS with MDTC   MANFCS with MDTC

Fig. 22 b Comparative results off SOR with CPID, MPID, MMRAS and MANFCS

The Rotor Speed of the system varies with the four controllers used in comparative results, speed will be zero for both CPID and MANFCS controllers from 0 sec to 30 seconds, whereas it will be zero for MPID and MMRAS controllers from 0 sec to 20 seconds. In the case of the MPID controller rotor speed will with positive and negative values, whereas for the other three controllers, it will be positive values only. Comparative results were shown in Fig. 22b and Table 2.

TABLE 2 COMPARATIVE RESULTS OF SOR WITH FOUR CONTROLLERS			
CPID with DTC		MPID with MDTC	
T in seconds	SOR in (radians/ second)	T in seconds	SOR in (radians/ second)
0 to 0.30	0	0 to 0.20	0
0.31 to 0.50	40	0.21 to 0.25	+5.50
0.51 to 0.60	40	0.25 to 0.30	+2.00
0.61 to 0.70	55	0.31 to 0.35	-6.50
0.71 to 0.80	55	0.36 to 0.40	-3.80
0.81 to 0.90	40	0.41 to 0.60	-2.00
0.91 to 0.95	40	0.61 to 0.65	+1.00
0.97 to 1.00	40	0.66 to 0.75	-7.50
1.01 to 1.20	0	0.76 to 0.80	+3.00

		0.81 to 0.90	-1.90
		0.91 to 1.00	-2.00
		1.01 to 1.10	-4.00
		1.11 to 1.20	0
MMRAS with MDTC		MANFCS with MDTC	
T in seconds	SOR in (radians/ second)	T in seconds	SOR in (radians/ second)
0 to 0.20	0	0 to 0.30	0
0.21 to 0.30	40	0.31 to 0.50	40
0.31 to 0.40	2	0.51 to 0.60	40
0.41 to 0.50	40	0.61 to 0.70	55
0.51 to 0.55	48	0.71 to 0.80	55
0.56 to 0.60	48	0.81 to 0.90	40
0.61 to 0.65	40	0.91 to 1.00	40
0.66 to 0.70	40	1.01 to 1.20	0
0.71 to 0.75	10		
0.76 to 0.78	10		
0.79 to 0.80	10		
0.81 to 0.90	40		
0.91 to 1.00	40		
1.01 to 1.15	0		
1.16 to 1.20	0		

5.3 Comparative results of EMT with four controllers

CPID with DTC   MPID with MDTC
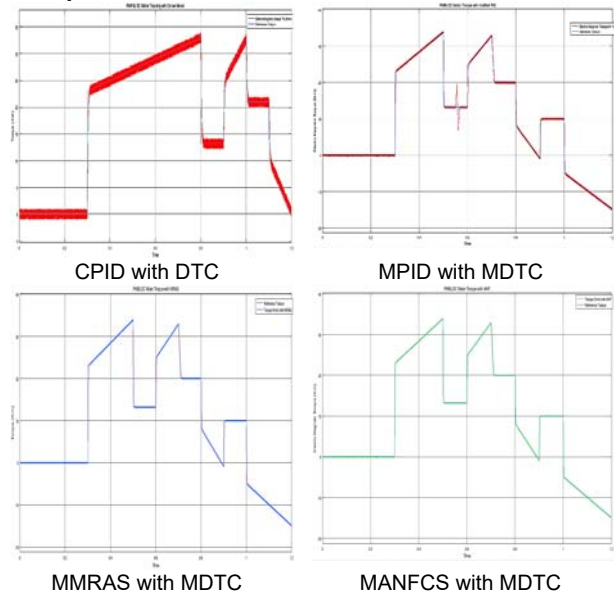
MMRAS with MDTC   MANFCS with MDTC

Fig. 22c Comparative results of torque with CPID, MPID, MMRAS and MANFCS

Fig. 22 Comparative Results of SOC, Speed and Torque with CPID, MPID, MMRAS and MANFCS

TABLE 3 COMPARATIVE RESULTS OF EMT WITH FOUR CONTROLLERS			
CPID with DTC		MPID with MDTC	
T in seconds	EMT in (Newton -meter)	T in seconds	EMT in (Newton- meter)
0 to 0.30	0	0 to 0.30	0
0.30 to 0.30	23	0.30 to 0.30	22
0.31 to 0.80	33	0.31 to 0.50	32
0.80 to 0.80	13	0.50 to 0.50	12
0.81 to 0.90	13	0.51 to 0.60	12
0.90 to 0.90	13	0.60 to 0.60	22
0.91 to 1.00	33	0.61 to 0.70	32
1.00 to 1.00	21	0.70 to 0.70	20
1.00 to 1.10	21	0.71 to 0.80	20
1.10 to 1.10	10	0.80 to 0.80	8
1.11 to 1.20	0	0.81 to 0.90	0
		0.90 to 0.90	10
		0.91 to 1.00	10
		1.00 to 1.00	-5
		1.01 to 1.20	-15

MMRAS with MDTC		MANFCS with MDTC	
T in seconds	EMT in (Newton -meter)	T in seconds	EMT in (Newton-meter)
0 to 0.30	0	0 to 0.30	0
0.30 to 0.30	22	0.30 to 0.30	22
0.31 to 0.50	32	0.31 to 0.50	32
0.50 to 0.50	12	0.50 to 0.50	12
0.51 to 0.60	12	0.51 to 0.60	12
0.60 to 0.60	25	0.60 to 0.60	25
0.61 to 0.70	32	0.61 to 0.70	32
0.70 to 0.70	20	0.70 to 0.70	20
0.71 to 0.80	20	0.71 to 0.80	20
0.80 to 0.80	8	0.80 to 0.80	8
0.81 to 0.90	0	0.81 to 0.90	0
0.90 to 0.90	10	0.90 to 0.90	10
0.91 to 1.00	10	0.91 to 1.00	10
1.00 to 1.00	-5	1.00 to 1.00	-5
1.01 to 1.20	-15	1.01 to 1.20	-15

Electro Magnetic Torque (EMT) varies with the four controllers used in the comparative study of the system, EMT value will be zero for all four controllers from 0 to 30 seconds, as in the case of conventional with direct torque the EMT values will be only positive i.e. for CPID, whereas for other three controllers i.e. for (MPID, MMRAS and MANFCS) with modified torque EMT values will be both positive and negative i.e. 0 to -15 will be same.

6. Conclusion

With regenerative braking system utilization in electric vehicles brake pads usage can be reduced, driving range can be extended and system maintenance cost can be reduced were proved by the usage of the proposed MANFCS controller by combining an adaptive neuro-based fully with a non-linear controller driven by BLDCM motor with modified torque and without changing the parameters. Variation in the load torque handled with the switching patterns (six switches) used in the proposed system, got simulation results proved in improving BSOC, SOR and Modified EMT of the system. A comparative study conducted by four controllers with direct and modified torque, on observation of results, can be concluded BLDCM motor performs well in regenerative braking operation and for low maintenance of the system. Good performance results were shown by the proposed system and observation of experiment results demonstrated achievement of dynamic performance, improvement in driving range and validating regenerative braking system for improved performance of electric vehicles.

Authors: Ms Shaik Ruksana Begum, Assistant Professor, EEE Department, Institute of Aeronautical Engineering, Hyderabad and Research Scholar in Koneru Lakshmaiah Education Foundation, Guntur, Email: ruksanabegam@iare.ac.in, Dr Loveswara Rao Burthi, Professor, EEE department, Koneru Lakshmaiah Education Foundation, Deemed to be University, Guntur, Email: loveswararao@kluniversity.in, Dr Shobha Rani Depuru, Professor, EEE Department, Institute of Aeronautical Engineering, Hyderabad, Email: d.shobharani@iare.ac.in.

REFERENCES

1 P. J. Grbovic, P. Delarue, P. Le Moigne, and P. Bartholomeus, "A bidirectional three-level dc-dc converter for the ultra-capacitor applications," *IEEE Trans. Ind. Electron.*, vol. 57, no. 10, pp. 3415–3430, Oct. 2010.
2 haligh, A.; Li, Z. Battery, ultracapacitor, fuel cell, and hybrid energy storage systems for electric, hybrid electric, fuel cell, and plug-in hybrid electric vehicles: State of the art. *IEEE Trans. Veh. Technol.* 2010, *59*, 2806–2814.
3 Ehsani, M.; Falahi, M.; Lotfifard, S. Vehicle to grid services: Potential and applications. *Energies* 2012, *5*, 4076–4090.
4 Falahi, M.; Chou, H.M.; Ehsani, M.; Xie, L.; Butler-Purry, K.L. Potential power quality benefits of electric vehicles. *IEEE Trans. Sustain. Energy* 2013, *4*, 1016–1023.
5 Shen, X.J.; Chen, S.; Li, G.; Zhang, Y.; Jiang, X.; Lie, T.T. Configure methodology of onboard supercapacitor array for recycling regenerative braking energy of URT vehicles. *IEEE Trans. Ind. Appl.* 2013, *49*, 1678–1686.
6 Yang, M.-J.; Jhou, H.-L.; Ma, B.-Y.; Shyu, K.-K. A cost-effective method of electric brake with energy regeneration for electric vehicles. *IEEE Trans. Ind. Electron.* 2009, *56*, 2203–2212
7 Khastgir, S. The Simulation of a Novel Regenerative Braking Strategy on Front Axel for an Unaltered Mechanical Braking System of a Conventional Vehicle Converted into a Hybrid Vehicle. In Proceedings of the 8th International Conference and Exhibition on Ecological Vehicles and Renewable Energies (EVER), Monte Carlo, Monaco, 27-30 March 2013; pp. 1-6.
8 Lahyani, A.; Venet, P.; Guermazi, A.; Troudi, A. Battery/supercapacitors combination in uninterruptible power supply (UPS). *IEEE Trans. Power Electron.* 2013, *28*, 1509–1522
9 Kuperman, A.; Aharon, I.; Malki, S.; Kara, A. Design of a semiactive battery-ultracapacitor hybrid energy source. *IEEE Trans. Power Electron.* 2013, *28*, 806–815.
10 Grbovic, P.J.; Delarue, P.; le Moigne, P.; Bartholomeus, P. The ultracapacitor-based regenerative controlled electric drives with power-smoothing capability. *IEEE Trans. Ind. Electron.* 2012, *59*, 4511–4522
11 Priewasser, R.; Agostinelli, M.; Unterrieder, C.; Marsili, S.; Huemer, M. Modeling, control, and implementation of DC-DC converters for variable frequency operation. *IEEE Trans.Power Electron.* 2014, *29*, 287–30.
12 Camara, M.; Dakyo, B.; Gualous, H. Polynomial control method of DC/DC converters for DC-bus voltage and currents management—Battery and supercapacitors. *IEEE Trans. PowerElectron.* 2012, *27*, 1455–1467.
13 Hredzak, B.; Agelidis, V.G.; Jang, M. A model predictive control system for a hybrid battery-ultracapacitor power source. *IEEE Trans. Power Electron.* 2014, *29*, 1469–1479.
14 Jung, H.; Conficoni, C.; Tilli, A.; Hu, T. Modeling and Control Design for Power Systems Driven by Battery/Supercapacitor Hybrid Energy Storage Devices. In Proceedings of the American Control Conference (ACC), Washington, DC, USA, 17–19 June 2013; pp. 4283–4288
15 Shaik, R.B., Kannappan, E. Application of Adaptive Neuro-Fuzzy Inference Rule-based Controller in Hybrid Electric Vehicles. *J. Electr. Eng. Technol.* 15, 1937–1945 (2020). https://doi.org/10.1007/s42835-020-00459-w.
16 Begam, Shaik Ruksana; Burthi, Loveswara Rao; Depuru, Shobha Rani, Adaptive Neuro-Fuzzy Sliding Mode Controller (ANF-SMC) to control speed, electromagnetic torque (EMT), Stator Current, and Back EMF using PMBLDC motor (PMBLDCM) in Electric Propulsion of Electric Vehicles, Przeglad Elektrotechniczny.2023, Vol. 2023 Issue 8, p49-62. 14p.